Engineering Structures 98 (2015) 163–173

Contents lists available at ScienceDirect

Engineering Structures

journal homepage: www.elsevier.com/locate/engstruct

Seismic behavior of SMA–FRP reinforced concrete frames under sequential seismic hazard

Adeel Zafar [a,b], Bassem Andrawes [c,*]

[a] Headquarters Frontier Works Organization, Pakistan
[b] School of Civil and Environmental Engineering, National University of Sciences and Technology, Pakistan
[c] Dept. of Civil Engineering, University of Illinois at Urbana-Champaign, USA

ARTICLE INFO

Article history:
Received 26 April 2013
Revised 26 January 2015
Accepted 22 March 2015

Keywords:
Shape memory alloys
Superelastic
Concrete
Fiber reinforced polymer
Aftershocks
Performance based design
Moment resisting frames

ABSTRACT

Accumulation of plastic deformation under excessive loads, is one of the most critical drawbacks in steel reinforced concrete structures. Permanent plastic deformation of steel rebars is among the main reasons for the disruption of the functionality of RC structures after major seismic events. It can also pose life threatening risks in case of strong aftershock occurrence. In an attempt to address the problem of excessive permanent deformations and their impact on the post-earthquake functionality of concrete moment resisting frame (MRF) structures, this paper studies analytically a new type of reinforcing bars made of fiber reinforced polymer (FRP) with embedded superelastic shape memory alloy (SMA) fibers. SMA–FRP reinforcement is characterized with both ductility and pseudo-elasticity which are two important characteristics that are sough in this study to enhance the ability of RC moment frames to withstand strong sequential ground motions (i.e. main shock followed by one or more aftershocks). In this study, experimentally validated SMA–FRP material models are used in structural level models to assess the performance of RC frame structures under seismic loading. Three-story, one-bay prototype RC MRFs, reinforced with steel and SMA–FRP composite reinforcements are first designed using performance based criteria and then subjected to incremental dynamic analysis under sequential ground motions. Comparison is drawn between steel and SMA–FRP reinforced frames based on accumulation of damage and residual drifts. Numerical results show superior performance of SMA–FRP composite reinforced MRF in terms of dissipation of energy and accumulation of lower residual drifts. Increased demands from the effects of aftershock causes accumulation of residual drifts in steel reinforced frames which is mitigated in SMA–FRP reinforced frame through re-centering capability.

1. Introduction

Traditional structural seismic design philosophy currently adopted by most seismic design codes is based on preventing the collapse of the structure during an earthquake through introducing the feature of ductility, which allows some level of damage to occur at specific components or regions (e.g. plastic hinges) in the structure. In the case of reinforced concrete (RC) structures, the damage is due to the crushing of concrete and the plastic deformation of steel reinforcement, which has been considered recently as one of the drawbacks of steel rebars. Excessive steel deformation (beyond yielding) in RC moment resisting frames (MRFs) for example often results in permanent residual drifts, which not only cause overall capacity degradation but also pose safety issues for the occupants even under gravity loads [1]. Several recent studies have focused on improving the post-earthquake functionality of RC structures through introducing the feature of re-centering. Various techniques have been proposed to introduce this feature to structures including the use of post-tensioned steel bars [2], enhancing post yield stiffness using steel fiber composite bars [3] and the use of superelastic shape memory alloy (SMA) rebars [4,5]. Although using SMA materials to provide RC structures with the ability to re-center is quite promising, it is faced with some challenges. For example, using large diameter SMA rebars that are not available commercially makes it cost prohibitive. In addition, research have shown that large diameter SMA rebars exhibit reduced hysteretic area and damping capability compared to small diameter wires [4,6]. This is primarily due to the accumulation of more distorted

* Corresponding author at: Dept. of Civil and Environmental Engineering, University of Illinois at Urbana-Champaign, USA.
E-mail addresses: zafar2@illinois.edu (A. Zafar), andrawes@illinois.edu (B. Andrawes).

http://dx.doi.org/10.1016/j.engstruct.2015.03.045
0141-0296/

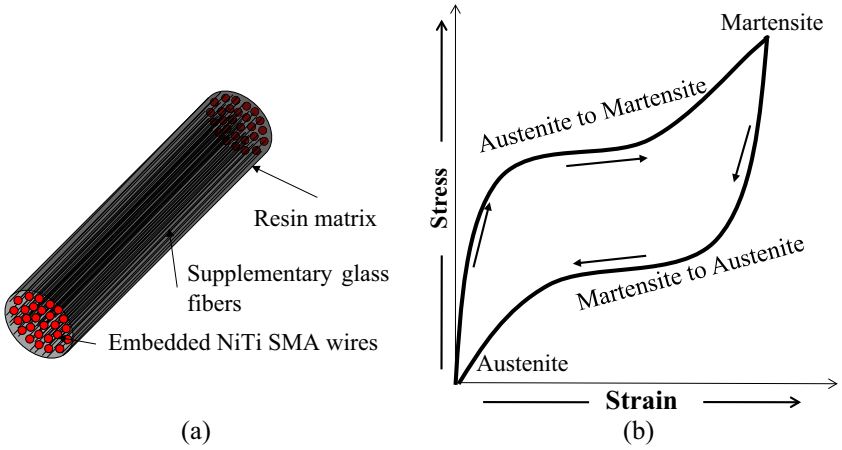

Fig. 1. Proposed SMA–FRP composite specimen. (a) Schematics of rebar. (b) Typical flag-shaped hysteresis of SMA.

martensite crystalline structure and inherent deficiencies which exist in larger diameter rods as compared to small diameter wires.

To address the previously discussed limitations in steel reinforcing bars using SMA wires instead of bars, the second author participated in a study which proposed the idea of using a new type of fiber reinforced polymer (FRP) composite known as shape memory alloy-FRP (SMA–FRP) as reinforcement for concrete structures [7]. The proposed reinforcement was sought as a mean to introduce the features of ductility and re-centering to RC structures. A schematic of the newly proposed composite rebar is shown in Fig. 1a. As illustrated in the figure, the proposed SMA–FRP reinforcing bar comprises polymeric resin reinforced with small diameter NiTi superelastic SMA fibers with or without supplementary conventional reinforcing fibers (e.g. glass, carbon, etc.). The nonlinear, yet pseudo-elastic behavior shown in Fig. 1b typical of superelastic SMA fibers [8] will allow SMA–FRP composite reinforcement to exhibit hysteretic and ductile behavior with minimal damage to the RC structure. The flag-shape hysteretic behavior of superelastic SMA is a direct result of a reversible stress-induced phase transformation between austenite and martensite phases. A more recent study by Zafar and Andrawes [9], explored in depth the manufacturing procedure and experimental testing behavior of the proposed SMA–FRP composite. In these previous studies, SMA–FRP has proven to be a promising alternative to both steel and FRP rebars, which deserves further investigation.

This paper focuses on investigating analytically, the performance of SMA–FRP rebars in RC MRF structures subjected to main shock–aftershock earthquake sequences and compare it with that of conventional steel rebars.

2. Main shock–aftershock seismic hazard

Structural seismic performance is often based on the response of structures to single major main shock seismic event. However, it is a common fact that aftershocks are often strong enough to cause serious damage and even collapse of structures, especially those which were already damaged during the main shock [10]. This study utilizes the effects of multiple seismic hazards as a way to assess level of damage expected in concrete MRFs. Accumulation of permanent drifts indicates permanent damage to the structure and could be utilized as a realistic way to incorporate effects of multiple earthquake hazards. Moreover, assessment of post-earthquake damage from multiple seismic events, allows examination of structural integrity for subsequent use. Recent earthquakes such as the Christchurch 2010 earthquake and the Tohoku 2011 earthquake have shown the devastating effects of aftershocks on RC buildings in terms of damage accumulation and permanent residual drifts due to plasticity of reinforcing steel [11,12]. Li and Ellingwood [10] investigated damage assessment of steel frame building under seismic sequence and found out that the characteristics (amplitude and frequency content) of the aftershocks have a significant influence on the structural damage pattern that develops as a result of the aftershock. Garcia et al. [13] studied the performance of highway bridges under scaled main shock–aftershock seismic sequence. They found that sequential dynamic analysis is an important analysis tool for evaluating structures ability to withstand shaking after amassing damage. They also found out that under scaled seismic sequence, the residual drift demands increase due to effects of aftershock. Recently, Garcia and Manriquez [14] performed a study which aimed at evaluating the effect of natural and artificial aftershock seismic events on steel framed buildings. Their study suggested incorporation of aftershock effects on structural response by utilizing natural earthquake records for multiple seismic hazard analysis because of their frequency content. Hatzigeorgiou and Liolios [15] also conducted a study which focused on the behavior of RC frames subjected to repeated ground motions. Their study showed that RC structures reinforced with steel are very much vulnerable to impact of aftershocks as they already are weakened due to damage accumulation and residual inter-story drifts (ID). The capability of the proposed SMA–FRP composite rebars in accumulating minimal damage after repeated cyclic loading is sought in this study to enhance the performance of RC MRF structures under sequential strong seismic events.

3. Numerical modeling of RC moment resisting frames

3.1. Element and structural modeling

Finite element program, OpenSees [16] which has been specifically designed for seismic analysis and earthquake simulations, was utilized to develop the composite constitutive models. A 2-D three-story, one-bay RC MRF was modeled to investigate the behavior of steel and SMA–FRP composite reinforcement. Fig. 2 shows details of frame configuration, layout of the reinforcement at the plastic hinge region, and cross sections of beam and columns utilized to develop the analytical model. The frame had a bay width of 6.5 m and story height of 3.6 m for all three stories. Nonlinear beam-column elements with fiber sections were used to model the moment resisting frame elements with distributed plasticity. In order to restrict the cost of material associated with use of NiTi SMA in the SMA–FRP composite, the reinforcing composite

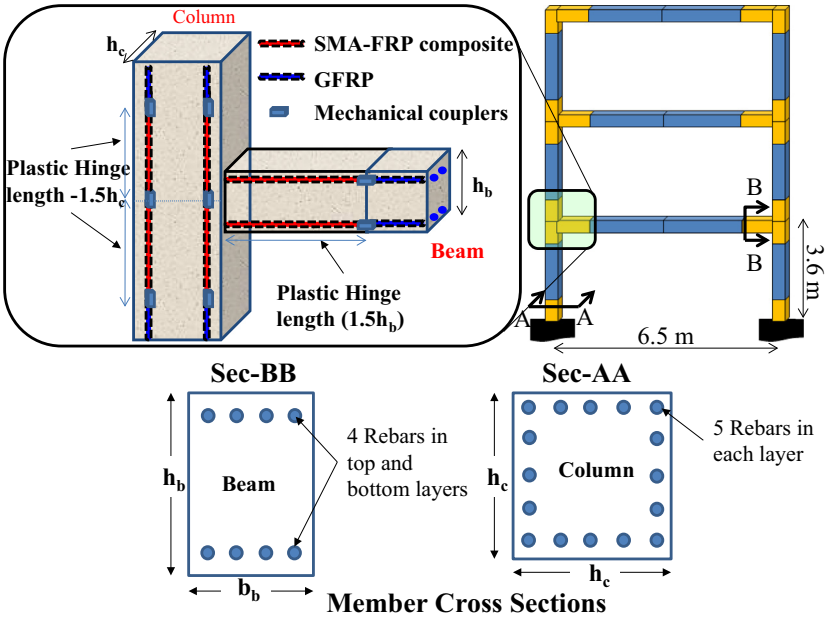

Fig. 2. Schematics of MRF configuration utilized in numerical modeling.

was only provided in the plastic hinge zones of MRF where high inelasticity is expected to develop. Rest of the frame was reinforced with conventional glass-FRP (GFRP) rebars. For frame analysis, it was assumed that SMA–FRP composite reinforcement constitutes of 65% fiber and 35% resin in terms of volumetric ratio. Perfect bond was also assumed between all reinforcement types and concrete material. This assumption is yet to be proven experimentally through structural testing. This study acts as preliminary investigation for exploring potential application for proposed SMA–FRP composite as primary reinforcement and its results might be altered if the bond-slip is found to be of significant importance in the future. More details related to the structural modeling technique adopted in this study can be found in [17].

3.2. SMA–FRP material modeling

The SMA–FRP composite considered in this study is reinforced with NiTi SMA wires with a diameter of 500 μm. These same wires were used in manufacturing the composite specimens that were tested in an earlier study by the authors [9]. Hence, their properties were predetermined. One of the significant differences between the proposed composite and conventional FRP composites typically used in civil structures is the type of resin used. Since SMA fibers are capable of reaching high strain levels (6–8%), it was essential to use high-ductility/elongation resin. High elongation resin host matrix allows for exploration of elongation potential of SMA wires which in turns allow improved energy dissipation through hysteretic action. A low straining resin would fail pre-maturely and thus would affect the overall ductile behavior of SMA–FRP composite. In the previously mentioned study, two specimens with 100% SMA reinforcement (Fully reinforced composite, FRC), named FRC-1 and FRC-2 and two specimens with hybrid reinforcement (Partially reinforced composite, PRC), named PRC-1 and PRC-2 were designed and manufactured. Experimental results showed that adding SMA fibers to the composite enhanced significantly the hysteretic energy dissipation capability of the composite while exhibiting decreased accumulated residual strains at the end of each cycle. On the other hand, addition of glass fibers in the SMA–FRP allowed the composite (PRC) to exhibit higher strength but lower ductility before the rupture of the glass fibers. This allows designers the flexibility to choose between both types of SMA–FRP composite based on the intended application. More details related to the manufacturing and testing of FRC and PRC specimens can be found in [9].

The experimental results from the composite testing were utilized to develop numerical material models for 100% SMA and hybrid composites. Table 1 shows detailed properties of each material obtained from experimental tests and utilized in developing the model. Fig. 3 shows schematic of stress–strain curves for each material utilized to develop numerical models for SMA–FRP composite. To develop stress–strain models of the composite, fiber section approach was used. SMA uniaxial material model available in OpenSees library was used to represent the behavior of SMA wire, elastic perfectly plastic (EPP) uniaxial material model was used to model the resin, while linear elastic material was used for depicting the behavior of glass fibers. Parallel material command was employed to link the epoxy and SMA/glass fiber material models, in which the strains are equal while stresses and stiffness's are additive.

Table 1
Material properties used in numerical models obtained from experimental tests.

Material	Property	Abvn.	Value
Concrete	Young's modulus	E_{conc}	26 GPa
	Ultimate strain	$\varepsilon_{Conc.}$	1.50%
	Compressive Strength	f'_c	30 MPa
Resin	Young's modulus	E_m	1.57 GPa
	Yield stress	Fy	32 MPa
SMA	Young's modulus	E_{SMA}	65 GPa
	Austenite to Martensite start stress	σ_{AMs}	500 MPa
	Austenite to Martensite finish stress	σ_{AMf}	510 MPa
	Martensite to Austenite start stress	σ_{MAs}	135 Mpa
	Martensite to Austenite finish stress	σ_{MAf}	145 Mpa
Glass fibers	Young's Modulus	E_f	86.7 GPa
	Rupture strain	ε_{Glass}	3.20%
Steel	Young's Modulus	E_s	200 GPa
	Yield Stress	Fy	420 MPa

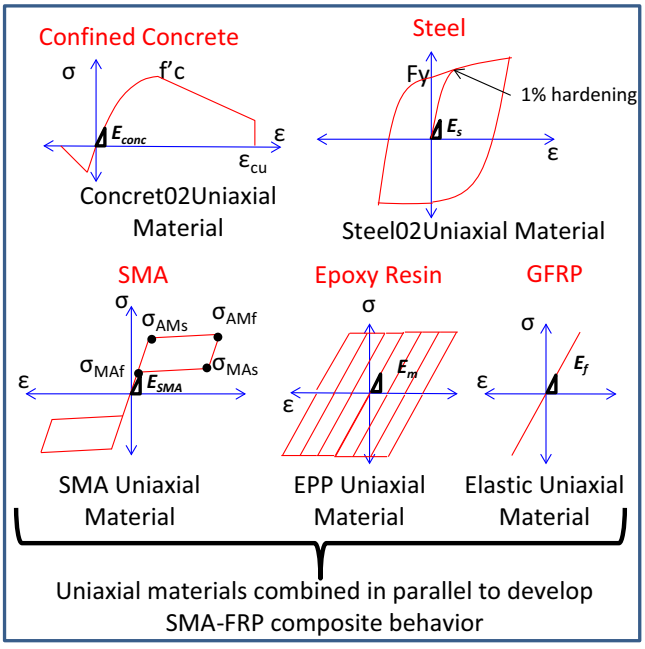

Fig. 3. Schematic of back bone stress–strain curves for various materials utilized to develop numerical models.

Fig. 4 shows comparison of experimental results and numerical model results for FRC-2 and PRC-1 composite specimens. Results show that the numerical models are able to depict the initial modulus and strength characteristics in addition to hysteretic behavior and accumulated residual strains of the composite for different strain levels and volumetric ratios. Numerical models are also able to capture the forward and reverse transformation associated with change of phase in SMA material. Even though the FRC and PRC specimens that are qualified experimentally have low fiber volume fractions (FVF) of SMA wires and glass fibers, the bars used in the analysis assumed much higher FVF (65%). The assumption that the developed constitutive models are able to numerically predict behavior of composite with FVF as high as 65%, is qualified notion as the models are able to capture the composite stiffness along with forward and reverse transformation associated with change of phase in SMA material. Because of compliance of numerical models with experimental results, even at low FVF, calibrated SMA–FRP composite material models were incorporated in SMA–FRP composite reinforced structural frame models for seismic analysis.

3.3. Concrete and steel models

Uniaxial material Concrete02 model, which considers concrete tensile strength, was used to represent the concrete behavior in the MRF models. The effect of confinement due to transverse reinforcement on the constitutive behavior of concrete was considered by adopting the model developed by Mander et al. [18]. No. 3 (9.5 mm-dia.) stirrups with 215 mm spacing were used to provide confinement to the core concrete. The spacing of stirrups for beam and column members was dictated by the shear demand for each target limit state computed during design process of MRF as explained later. For unconfined concrete, a compressive strength of 30 MPa and a strain of 0.2% corresponding to peak compressive strength were assumed. Base model for confinement was developed for steel reinforcement and was kept the same for sake of consistency and comparison with SMA–FRP reinforced sections. The steel behavior was described using Steel02 model predefined in OpenSees, which is based on the Giuffre–Menegotto–Pinto model with isotropic strain hardening [19]. Grade 60 steel with modulus of elasticity of 200 GPa was used to design the structure.

4. Performance based design of moment resisting frames

Performance based design approach was used for designing the MRF with steel and SMA–FRP composite. This seismic design approach has been considered recently in lieu of conventional force-based design [20]. Performance based engineering (PBE) involves use of peak lateral displacement demands and capacities as mean to assess the structures performance during a seismic event. Generally, performance objectives are pre-quantified by the inter-story drift ratio (IDR) limit, which has become a common earthquake demand parameter (EDP) that is used for assessing the damage in structures [1]. IDR is defined as the ratio between maximum relative displacement of two immediate floor levels and the height of that floor. Present seismic design practice advocates use of displacement-based criteria bounded by certain performance limit states (LS). FEMA-273 [21] defines these limit states in terms of three structural performance levels, namely immediate occupancy (IO), life safety/damage control (LS) and collapse prevention (CP). Since the focus of this study is to develop a new SMA-based composite reinforcement which can exhibit better performance at higher ductility demands and damage during sequential seismic events, collapse prevention, which is generally associated with severe structural damage was selected as limit state.

Since IDR values larger than 4% may result in irreparable structural damage or collapse [22], the maximum IDR limit state adopted in this study, was 4%. A limit state of 3% IDR was also studied to examine the performance of the new reinforcement under various demand levels. Displacement based design approach was adopted by incorporating capacity spectrum method (CSM) as defined by Applied Technology Council (ATC-40) [23]. The procedure compares the capacity of the structure (in the form of push-over curve up to target IDR) with the demands on the structure (in the form of response spectrum). The graphical intersection of the two curves dictates the design of the frame by approximating

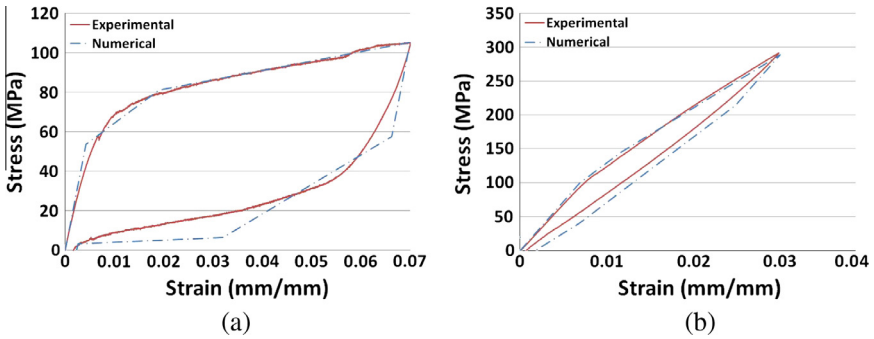

Fig. 4. Comparison of stress strain curves of experimental results and numerical models (a) FRC-2 composite (b) PRC-1 composite.

the response. In order to imitate a nonlinear response of the MRF, effective damping values are used to reduce the linear elastic response spectrum (LERS) with 5% equivalent viscous damping ratio to inelastic response spectra (IRS). The effective damping ratios can be related to ductility ratios for various characteristics of hysteretic behavior and can be used to determine spectral reduction factors. The original procedure as an evaluation tool is explained in detail in ATC-40. Many researchers [24,25] have suggested modification to the ATC-40 procedure for adaptation as design tool. A schematics representing the design procedure using capacity spectrum method is depicted in Fig. 5. After initial estimation of cross sections and reinforcement ratio, the frame is analyzed to obtain pushover curve and dynamic response characteristics such as fundamental elastic period, modal participation factor and effective modal.

The pushover curves which were converted to capacity spectrum in acceleration vs. displacement format (A–D) were then matched up with inelastic response spectrum in A–D format for target IDR. The elastic response spectrum was developed based on the International Building Code (IBC-2006) for a high seismic zone with site classification B in California. The mapped spectral acceleration for short period (S_s) was 1 g and mapped spectral acceleration for 1-s period (S_1) was 0.5 g. The frame is then redesigned to obtain capacity spectrum which would exactly intersect inelastic response spectrum at target IDR. This iterative process not only requires change in member sizes but also in reinforcement ratio.

The final reinforcement ratios for beam and columns in both frames reinforced with steel and SMA–FRP are shown in Table 2. The selected beam and column dimensions for MRF designed for 3% IDR demand were 300 × 525 mm and 475 × 475 mm, respectively. For MRF designed for 4% IDR, the beam and column dimensions were 300 × 500 mm and 450 × 450 mm, respectively.

5. Sequential seismic input

Natural ground motion records from six earthquakes were chosen as seismic input for sequential nonlinear time history analysis. The sequential records i.e. the main shocks and the aftershocks were recorded by same station and in same direction. The characteristics of the seismic sequences used in this study are shown in

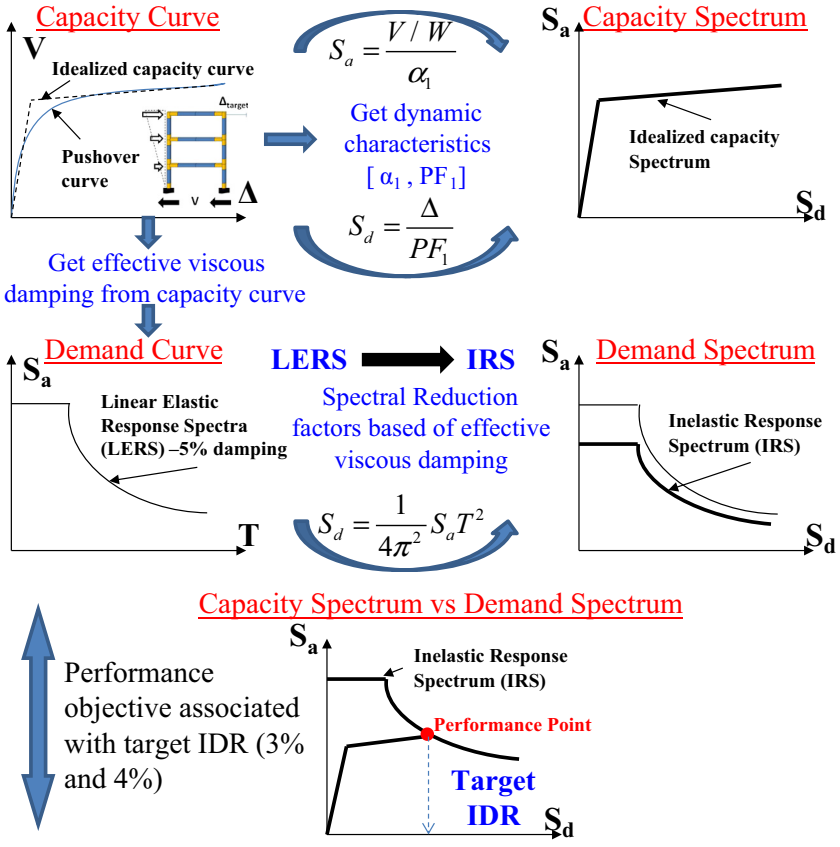

Fig. 5. Schematics of methodology adopted for design of MRFs.

Table 2
Reinforcement ratio for the designed column and beam cross-sections.

Performance limit state	Reinforcement ratio (ρ-%)				Fundamental period (s)		Ultimate strain of confined concrete (%)
	Beam		Column		Steel	SMA–FRP	
	Steel	SMA–FRP	Steel	SMA–FRP			
3 % IDR design (MRF-3%)	1	1.5	2.56	3.8	0.46	0.52	1.4
4% IDR design (MRF-4%)	0.9	1.4	2.56	3.52	0.49	0.57	1.6

Table 3
Sequential seismic input and their characteristics.

Earthquake	Record station	Sequence	Date	Magnitude (M_w)	PGA (g)	Duration ratio (main/after)
1979 Imperial Valley	5055 Holtville P.O.	Main	10/15/1979	6.6	0.601	1.57
		After	10/15/1979	5.2	0.12	
1980 Mammoth Lake	54099 Convict Creek	Main	5/25/1980	6.1	0.441	1.22
		After	5/25/1980	6	0.178	
1983 Coalinga	Pleasant valley pump yard-1162	Main	5/2/1983	6	0.591	2.19
		After	7/22/1983	5.3	0.602	
1986 Chalfant Valley	54428 Zack Brothers Ranch	Main	7/21/1986	5.9	0.447	0.37
		After	7/31/1986	6.3	0.064	
2010 Christchurch	Christchurch Botanic Garden (CBG)	Main	9/3/2010	7.1	0.1494	2.47
		After	2/21/2011	6.3	0.529	
2011 Tohoku	FKS 013	Main	3/11/2011	9	0.36	1.01
		After	4/7/2011	7.4	0.0966	
2010 Christchurch	Christchurch Cathedral College (CCC)	Main	9/3/2010	7.1	0.149	2.09
		After-1	9/7/2010	5.13	0.126	
		After-2	10/18/2010	5.03	0.0813	
		After-3	12/25/2010	4.9	0.216	

Table 3. The Christchurch event from CCC recording station is a 4-event sequence while all others are 2-event sequences.

One of the critical ground motion parameters that controls the extent of damage caused by the ground motion is the duration. Numerous definitions of ground motion record durations have been proposed, but for this research 'significant duration' was defined as the time interval over which a portion of the total energy integral is accumulated. The accumulation of energy in earthquake record can be computed as the integral of the square of the ground acceleration and this quantity is related to Arias intensity, AI [26] given by the following expression:

$$\mathrm{AI} = \frac{\pi}{2g}\int_0^{tr} a^2(t)dt \tag{1}$$

where $a(t)$ is the acceleration time history and tr is the total duration of the record. Generally, the significant duration is assumed equal to the build-up of the Arias intensity between two arbitrary limits, which were assumed to be 5% and 95% [27]. Since the ground motion records are required to be scaled for analysis (discussed later), use of significant duration seems more appropriate and justified. Based on above mentioned definition, ratios between durations of main shock and aftershock records are shown in Table 3 for all the records. Duration ratio for the earthquake record from Christchurch Cathedral College (CCC) with 4-event sequence has been computed by comparing the total duration from all three aftershocks with that of the main shock.

6. Analysis technique

The seismic response of the examined MRFs was investigated using sequential incremental dynamic analysis (IDA). IDA method involves subjecting a structural model to multiple levels of intensity by scaling the ground motion record [28]. IDA technique allows focusing on the frequency content of the ground motion as the whole record is scaled with same intensity level. The primary goal of IDA technique is to quantify the reserve capacity of the structure against target performance level. In step-1 of the analysis, the main shock record was scaled incrementally using scaling factors (S.F.) until the target IDR (3% or 4%) is reached in both designed MRFs with steel and SMA–FRP reinforcement. In the subsequent analysis in step-2, the scaled main shock (from step-1) and the original aftershocks were combined together to form a single sequential ground motion record and was again applied to each MRF. A time gap was applied between each scaled main shock and aftershock record of 50 s to curb any transient vibration. The aftershock part of the sequential record was then scaled to different intensity levels until the scaled sequential ground motion record again causes 3% and 4% IDR in the MRF. The analysis technique being used in this study is further explained in the illustration presented in Fig. 6. For the case with 4-event sequence, similar analysis procedure was adopted as mentioned earlier. After scaling the main shock to a specific target IDR, first aftershock was scaled to result in the same IDR. The damaged frames were again subjected to 2nd and 3rd aftershock sequences till the target IDR LS is achieved. Drift time history for steel and SMA–FRP reinforced frames were developed to determine the corresponding PGA which would satisfy the target performance level (3% and 4% IDR). Accumulations of residual IDR in frames were also recorded for each earthquake sequence.

7. Results and discussion

7.1. Sample IDR time histories

Fig. 7 shows the IDR time history of both MRF-4% when subjected to a sample case of Tohoku earthquake sequential records. Main shock from Tohoku was required to be scaled to a PGA of 2.27 g and 1.55 g to cause 4% IDR for steel and SMA–FRP reinforced frames, respectively. Because of inherent higher stiffness and lower fundamental period, steel reinforced frame required higher seismic input (PGA/scaling factor) from main shock record to reach to 4% IDR as compared to SMA–FRP reinforced frame. Hereafter, the scaled main shock was kept unchanged while the aftershock was scaled till both frames again experienced 4% IDR. The aftershock from Tohoku earthquake had to be scaled to a PGA of 1.29 g and 1.61 g to reach the target performance limit state for steel and SMA–FRP reinforced frames, respectively. It is worth noting that steel reinforced frame accumulated 0.47% residual IDR from main shock and this permanent drift increased to 0.84% by the end of aftershock. This net residual IDR increase by 79% is due to sequential earthquake influence. On the other hand, because of re-centering capability of SMA composite reinforcement, there was no accumulation of permanent damage or drift in SMA–FRP reinforced frame.

Fig. 8 shows response of MRF-4% for the two reinforcement types to the 4-event sequence from Christchurch earthquake.

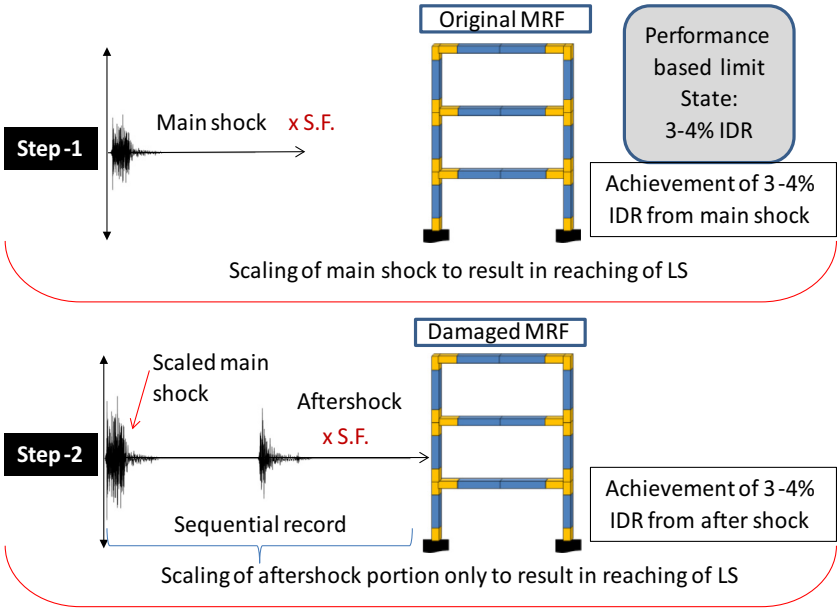

Fig. 6. Illustration of sequential seismic analysis technique.

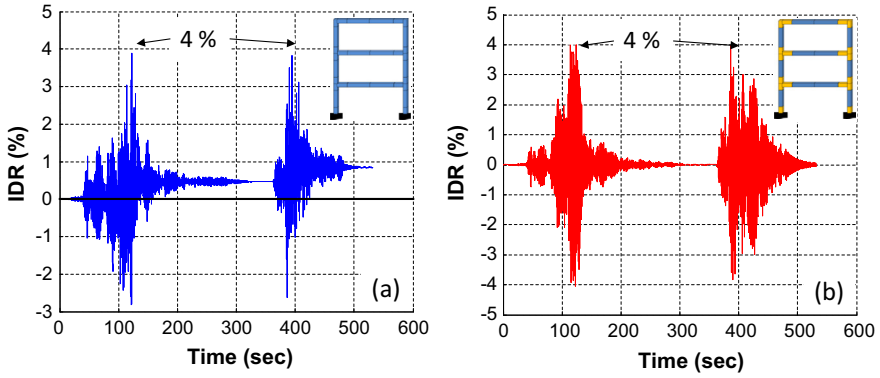

Fig. 7. IDR time history response of MRF-4% subjected to Tohoku sequence event: (a) Steel. (b) SMA–FRP reinforcement.

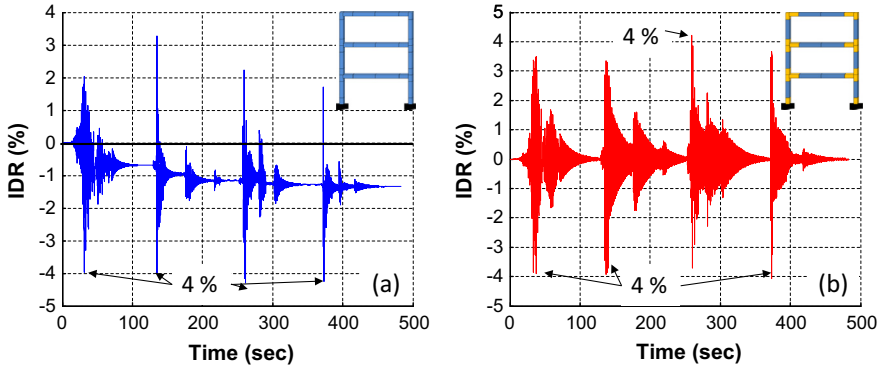

Fig. 8. IDR time history response of MRF-4% subjected to CCC 4 sequence event: (a) Steel. (b) SMA–FRP reinforcement.

Results from analysis show accumulation of permanent drift in steel reinforced frame when subjected to multiple sequential records each scaled to cause 4% IDR. After the fourth ground motion record in Christchurch sequence (After-3), the residual IDR accumulated was found to be 1.25%. This is an increase of 229% in permanent deformation as compared to main shock response. It has been observed that the accumulation of residual drifts after each record makes the steel reinforced frame vulnerable and prone to collapse even with smaller intensity aftershock. Analysis results from other remaining sequential ground motion

records showed similar behavior as shown in sample cases of Tohoku earthquake and Christchurch CCC 4-event sequence earthquake records.

7.2. Comparison of accumulation of residual IDR

Figs. 9 and 10 show comparison of accumulated residual IDR from all main shock and sequential records considered in the study for both MRF-3% and MRF-4%, respectively. Maximum percentage increase in residual IDR in case of 2-event sequence was observed for Christchurch earthquake sequence when considering aftershock effects. In case of MRF-3%, this increase in IDR was 117% while it was 123% for MRF-4% case. For 4-event sequence, the increase in IDR was 224% and 229% for MRF-3% and MRF-4%, respectively. Average residual IDR for main shock and aftershocks from all records in case of MRF-3% was 0.37% and 0.65%, respectively. This amounts to an increase of 75.6% in accumulation of residual IDR compared to the main shock only case. Similarly, for MRF-4%, an average residual IDR for main shock and aftershocks from all records was found to be 0.6% and 1.12%, respectively. This amounts to an increase of 86.6% in accumulation of residual IDR compared to the case of main shock only. Comparing accumulation of residual IDR from steel reinforced MRF-3% and MRF-4% revealed increase of 14.5% in residual IDR for MRF-4% compared to MRF-3%. This increase is deemed high considering that the increase in design limit state was only by 1% drift, going from 3% to 4% IDR.

7.3. Reduction factor

The accumulation of residual permanent drifts in steel reinforced frame due to seismic sequences resulted in decreased PGA needed to reach 3% and 4% IDR. This multiplicity earthquake effect is quantified in terms of reduction factor (%) once compared to SMA–FRP reinforcement type. This reduction is a function of $(PGA)_{Steel}/(PGA)_{SMA-FRP}$ which causes 3% and 4% IDR and corresponds to reduction in PGA required, going from main shock to aftershock for the same earthquake. Eq. (2) represents the definition of reduction factor used in this study:

$$\text{Reduction factor} = 1 - \frac{[(PGA)_{Steel}/(PGA)_{SMA-FRP}]_{Sequence}}{[(PGA)_{Steel}/(PGA)_{SMA-FRP}]_{Main}} \quad (2)$$

This reduction factor allows taking into account the phenomena of residual IDR accumulation and thus requiring lesser PGA for steel reinforced frame to reach target performance levels. Reduction factors for MRF-3% and MRF-4% are graphically shown in Fig. 11 once subjected to the selected sequential inputs.

It is evident from results that MRF-4% exhibits more reduction factor as compared to MRF-3% in all case considered for this study. Maximum increase in reduction factor between MRF-3% and MRF-4% case was observed for Tohoku earthquake record which exhibited 104.5% increase. As mentioned earlier, reduction factor is able to quantify reduction in capacity of steel reinforced frame as compared to SMA–FRP reinforced frame. Thus larger the reduction factor, more damage to the structure due to multiplicity of earthquake affect. Maximum reduction factor was observed for 4-event Christchurch earthquake sequence for both MRF-3% (43%) and MRF-4% (49%).

7.4. Correlation between duration ratio and reduction factor

As mentioned earlier, the sustenance of drifts and magnitude of residual drift depends on the duration of shaking and number of cycles. A ratio between durations of main shock and aftershock records was computed for all the records as shown in Table 3. This duration ratio of any sequential record less than one implies longer aftershock record and more number of cycles as compared to main shock, thus more potential to accumulate damage after

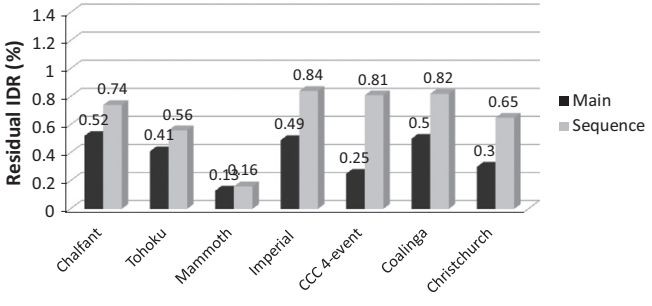

Fig. 9. Accumulation of residual IDR in MRF-3%.

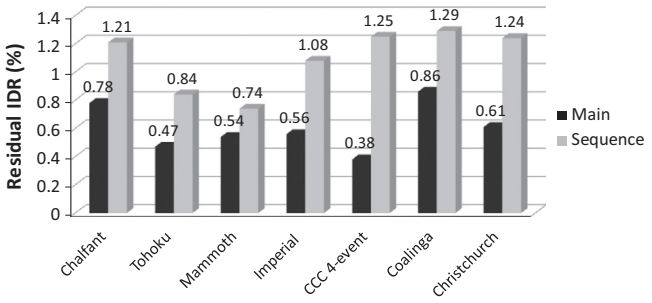

Fig. 10. Accumulation of residual IDR in MRF-4%.

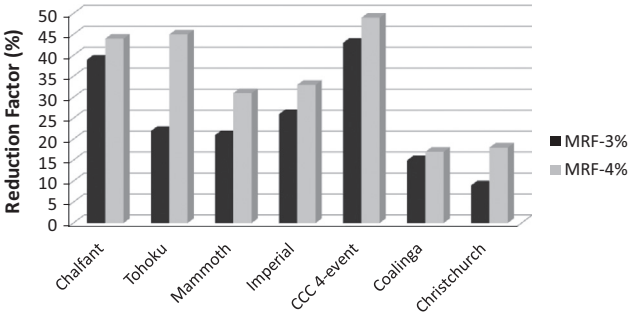

Fig. 11. Reduction factors for MRF-3% and MRF-4%.

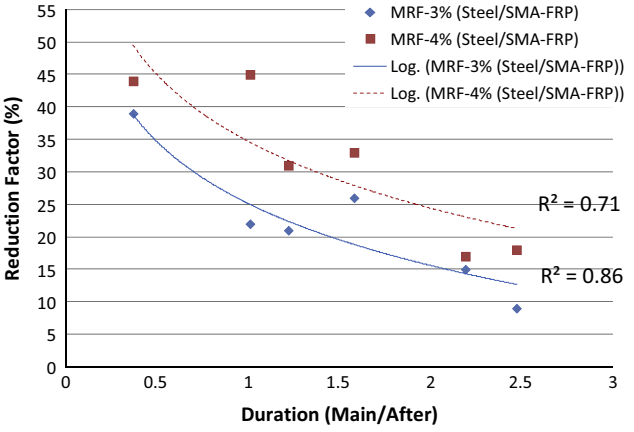

Fig. 12. Correlation between duration ratio and reduction factor.

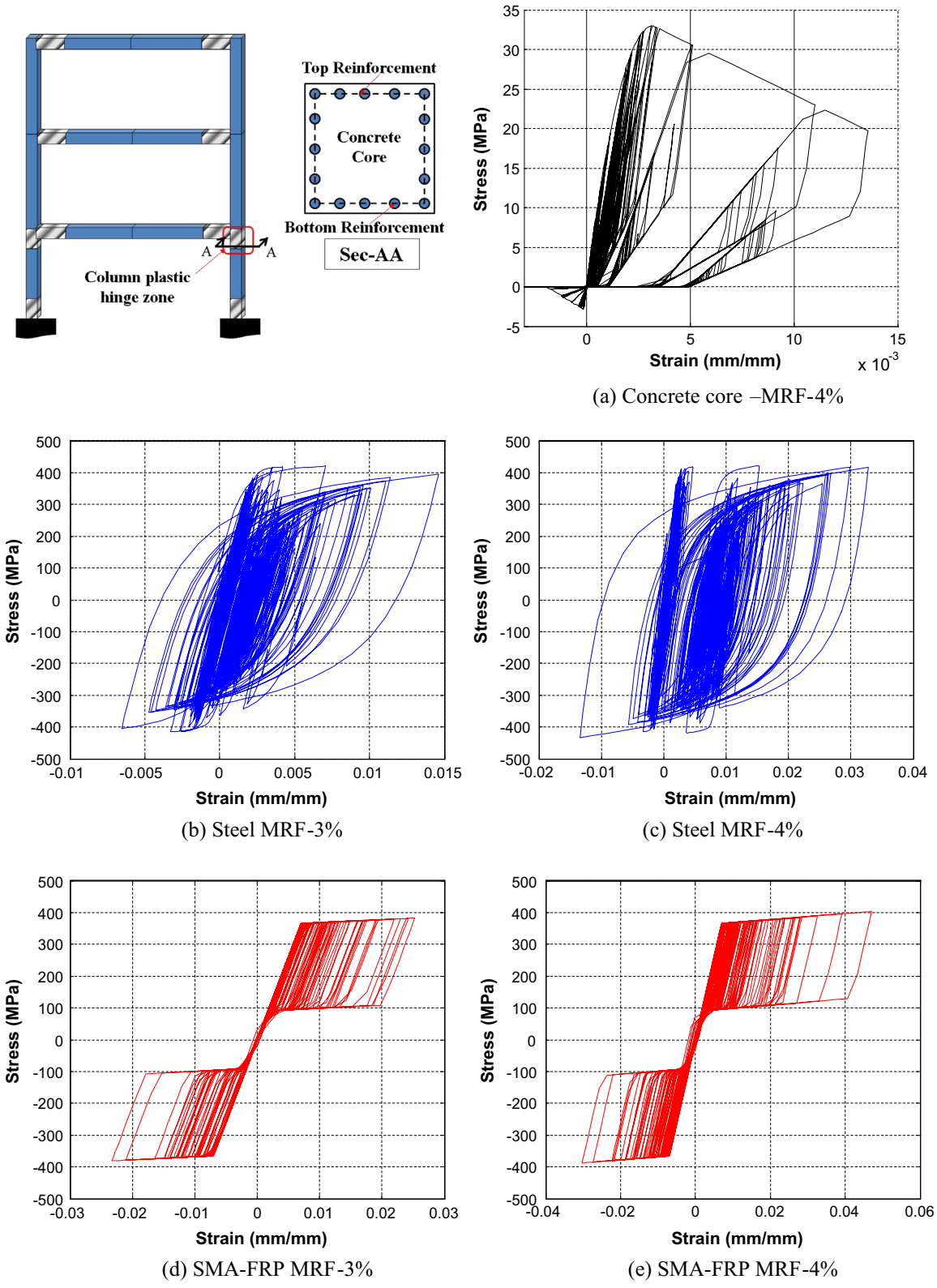

Fig. 13. Stress–strain plots of MRF subjected to Tohoku earthquake sequential records: (a) Core concrete in base column in MRF-4%. (b) Steel reinforced MRF-3%. (c) Steel reinforced MRF-4%. (d) SMA–FRP reinforced MRF-3%. (e) SMA–FRP reinforced MRF-4%.

an initial main shock event. A correlation between the duration ratio and reduction factor was formulated for each sequence for SMA–FRP in comparison with steel reinforcement for both MRF-3% and MRF-4%. Fig. 12 shows the relationship between duration ratio and reduction factor (two unit less values) for both MRF-3% and MRF-4% scenarios.

The results from Fig. 12 point out that SMA–FRP reinforced frame exhibits superior performance in relation to steel reinforced

frame. For every earthquake sequence considered, the reduction factor for steel/SMA–FRP was greater for MRF-4% as compared to MRF-3%. A logarithmic tread line was plotted for both MRF-3% and MRF-4% cases as seen in Fig. 12, with R^2 (square of residuals) value of 0.85 and 0.71, respectively. Fig. 12 also points out the fact that as the duration ratio increases, the reduction factor decreases. This is true for both 3% and 4% IDR cases, however the slope and shape of the curve changes. In other words, if the duration factor is less (meaning the aftershock is longer and has more cycles), more damage (quantified as reduction factor) would be exhibited by steel reinforced frame. This proves that the seismic damage for multiple earthquakes is higher than that of single ground motion. Thus traditional seismic design process, which essentially is based on isolated design ground motion, is inadequate to achieve dependable estimation of permanent residual drifts and damage.

7.5. Response at material level

For the purpose of illustration, a plot of material stress–strain is shown in Fig. 13 for MRF-3% and MRF-4% when subjected to Tohoku earthquake record sequence. Fig. 13(a) shows material response of core concrete at the same plastic hinge location in the column for steel reinforced MRF-4%. The response shows core concrete reaching ultimate strain of 0.0137 mm/mm. In Fig. 13(b), stress–strain plot of steel reinforcement of the 1st story column at the location of plastic hinge in MRF-3% is shown. Maximum strain experienced by the steel reinforcement is 1.4%. Steel material response shows accumulation of residual strains due to permanent damage to the RC column and MRF. The material response of SMA–FRP shows typical flag shape hysteresis with re-centering capability. Fig. 13(c) shows stress–strain plot of steel reinforcement in MRF-4% at the same location. The maximum strain exhibited is 3.3% which is an increase of 57.5% from the MRF-3% case. Similarly, in Fig. 13(d and e), stress–strain plot of SMA–FRP reinforcement in MRF-3% and MRF-4% are shown. Maximum strain exhibited by SMA–FRP reinforcement for MRF-4% is 4.7% which is an increase of 80.7% from MRF-3% which exhibited 2.6% strain in the reinforcement. It is worth noting that since EPP model, which was used to represent the resin matrix in the model, was combined in parallel with SMA material, a slight variation in stiffness was observed in composite behavior during compression to tension cycles, as seen in Fig. 13(d and e).

8. Conclusions

This study focused on the use of SMA–FRP composite as a new reinforcement for RC MRFs to improve their seismic behavior and reduce their residual drifts after earthquake sequences. Numerical models for SMA–FRP composite material were developed and validated using experimental data while showing good correlation. These numerical models were then implemented in global structural models to investigate the seismic response of MRFs reinforced with the proposed reinforcement. Prototype MRFs were designed using CSM and performance based criteria for steel and SMA–FRP reinforcements. Both MRFs were designed for two performance levels; 3% and 4% IDR and were subjected to sequential seismic input. IDA technique was used to study the seismic behavior of the frame under suite of sequential earthquake records. The following are the main conclusions of the study:

- Irrespective of the earthquake record, it was evident that the seismic sequence (i.e. main shock followed by one or more aftershocks) leads to increased residual IDR in steel reinforced frames due to yielding and permanent damage (plasticity) compared to the case when only main shock is considered.
- Under main shocks only, the frame with steel reinforcement initially experienced 3% and 4% IDR at higher PGA as compared to the frame reinforced with SMA–FRP because of its higher initial stiffness. However, when steel starts yielding, the steel reinforced frame experiences residual IDR as opposed to frame with SMA–FRP composite reinforcement. Because of accumulation of damage from the main shock, a steel reinforced frame ended up requiring smaller PGA to reach the target performance limit state as compared to frame reinforced with SMA–FRP composite.
- The frame with steel reinforcement was able to dissipate more hysteretic energy as compared to the frame with SMA–FRP reinforcement, but at the cost of permanent residual IDR. Accumulation of permanent drifts and vulnerability of steel reinforced frame to aftershock was quantified using reduction factors.
- MRF-3% with steel reinforcement experienced reduction in capacity (as high as 43%) when subjected to various seismic sequences as compared to SMA–FRP reinforced frame. In other words, steel reinforced MRF-3% was required to withstand as low as 43% lesser seismic demand (PGA) as compared to SMA–FRP MRF-3% for the seven ground motion sequences. This reduction further increased for the 4% IDR performance limit state (as high as 49%) showing greater vulnerability of steel reinforced frame to aftershock as compared to SMA–FRP reinforced frames.
- A relationship between duration for earthquake sequences and reduction factors was developed. Results showed that as the duration ratio increases, the reduction factor decreases for all the cases and scenarios.
- This study showed that the use of SMA–FRP rebars in the plastic hinge zones of MRFs reduces significantly the accumulation of permanent damage and residual drifts compared to steel reinforced MRFs, thus improving the overall performance of frame under sequential seismic hazard. Results also showed that use of SMA–FRP rebars in plastic hinge zones allows structure to dissipate energy through hysteretic action of SMA along with providing it with the ability to re-center. This re-centering is an essential feature for structures to mitigate the effects of sequential earthquake hazards.

References

[1] Elnashai AS, Luigi DS. Fundamentals of earthquake engineering. New York: Wiley; 2008.
[2] Nakahara H, Saniko K, Esaki F. Experimental study for developing self-centering RC structural frames with column yielding mechanism. J Struct Constr Eng AIJ June 2008;73(628):957–64.
[3] Fahmy MFM, Wu Z, Wu G, Sun Z. Post-yield stiffnesses and residual deformations of RC bridge columns reinforced with ordinary rebars and steel fiber composite bars. Eng Struct 2010;32:2969–83.
[4] Saiidi M, Zadeh M, Ayoub C, Itani A. A pilot study of behavior of concrete beams reinforced with shape memory alloys. J Smart Mater Civil Eng ASCE 2007;19(6):454–61.
[5] Nehdi M, Alam MS, Youssef MA. Development of corrosion-free concrete beam column joint with adequate seismic energy dissipation. Eng Struct 2009;32:2518–28.
[6] Speicher MS, DesRoches R, Leon RT. Experimental results of a NiTi shape memory alloy SMA)-based recentering beam-column connection. Eng Struct 2011. http://dx.doi.org/10.1016/j.engstruct [04.018].
[7] Wierschem N, Andrawes B. Superelastic SMA–FRP composite reinforcement for concrete structures. J Smart Mater Struct 2010;19:13.
[8] Naito H, Sato J, Funami K, Matsuzaki Y, Ikeda T. Analytical study on training effects of pseudoelastic transformation of shape memory alloys in cyclic loading. J Intell Mater Syst Struct 2001;12:295–300.
[9] Zafar A, Andrawes B. Fabrication and cyclic behavior of highly ductile superelastic shape memory composites. ASCE J Mater Civ Eng 2013. http://dx.doi.org/10.1061/(ASCE)MT.1943-5533.0000797.
[10] Li Q, Ellingwood BR. Performance evaluation and damage assessment of steel frame buildings under main shock–aftershock sequences. Earthq Eng Struct Dynam 2007;36:405–27.

[11] Weng Kam Y, Pampanin S. The seismic performance of RC buildings in the 22 February 2011 Christchurch earthquake. Struct Concr 2011;12(4). http://dx.doi.org/10.1002/suco.20110004.
[12] Nishiyama I, Okawa I, Fukuyama H, Okuda Y. Building damages by the 2011 off the Pacific coast of Tohoku earthquake and coping activities by NILIM and BRI collaborated with the administration. Report by National Institute for Land & Infrastructure Management (NILIM) and Building Research Institute (BRI).
[13] Garcia JR, Moreno JY, Maldonado IA. Evaluation of existing Mexican highway bridges under mainshock–aftershock seismic sequences. In: Proceedings of the 14th world conference on earthquake engineering. Paper 05-02-0090. China; 2008.
[14] Garcia JR, Manriquez JCN. Evaluation of drift demands in existing steel frames under as-recorded far-field and near-fault main shock–aftershock seismic sequences. Eng Struct 2011;33:621–34.
[15] Hatzigeorgiou GD, Liolios AA. Nonlinear behaviour of RC frames under repeated strong ground motions. Soil Dyn Earthq Eng 2010;30:1010–25.
[16] Mazzoni S et al. Open system for earthquake engineering simulation (OpesSees). OpenSees command language manual. Berkeley (CA): Pacific Earthquake Engineering Research Center, University of California; 2009.
[17] Zafar A, Andrawes B. Incremental dynamic analysis of concrete moment resisting frames reinforced with shape memory composite bars. J Smart Mater Struct 2012;21:025013–25014.
[18] Mander JB, Priestley JN, Park R. Theoretical stress strain model for confined concrete. J Struct Eng 1988;114(8).
[19] Menegotto M, Pinto method of analysis for cyclically loaded RC plane frame including changes in geometry. Preliminary Report IABSE, vol 13; 1973. p. 15–22.
[20] Federal emergency management agency. Next generation Performance based seismic design guidelines. Report FEMA 445. Washington (DC); 1996.
[21] Federal emergency management agency. NEHRP guidelines for the seismic rehabilitation of buildings. Report FEMA 273. Washington (DC); 1997.
[22] Sozen MA. Review of earthquake response of reinforced concrete buildings with a view to drift control. State-of-the-Art in Earthquake Engineering, Turkish National Committee on Earthquake Engineering, Istanbul, Turkey; 1981. p. 383–418.
[23] ATC-40. Seismic evaluation and retrofit of concrete buildings, vol. 1. Applied Technology Council, Redwood City (California); 1996.
[24] Freeman SA. Development and use of capacity spectrum method. In: Proceedings of the 6th US national conference on earthquake engineering. Seattle, EERI, Oakland, California; 1998.
[25] Xue Q, Wu CW. Preliminary detailing for displacement based seismic design for buildings. Eng Struct 2006;28:431–40.
[26] Arias A. A measure of earthquake intensity. In: Hansen R, editor. Seismic design for nuclear power plants. Massachusetts: MIT Press; 1970. p. 438–83.
[27] Husid LR. Characteristicas de terremotos. Analis general. Revista del IDIEM, Santiago, vol. 8; 1969. p. 21–42.
[28] Vamvatsikos D, Cornell AC. Incremental dynamic analysis. Earthq Spectra 2001;20:523–53.